Inorg. Chem. **2008**, *47*, 2024−2032

Electron Transfer Mechanism and Photochemistry of Ferrioxalate Induced by Excitation in the Charge Transfer Band

Jie Chen, **Hua Zhang**, **Ivan V. Tomov**, **and Peter M. Rentzepis***

Department of Chemistry, University of California, Irvine, California 92697

Received August 22, 2007

The photoredox reaction of ferrioxalate after 266/267 nm excitation in the charge transfer band has been studied by means of ultrafast extended X-ray absorption fine structure (EXAFS) analysis, optical transient spectroscopy, and quantum chemistry calculations. The Fe−O bond length changes combined with the transient spectra and kinetics have been measured and in combination with ultrahigh frequency density functional theory (UHF/DFT) calculations are used to determine the photochemical mechanism for the Fe(III) to Fe(II) redox reaction. The present data and the results obtained with 266/267 nm excitations strongly suggest that the primary reaction is the dissociation of the Fe−O bond before intramolecular electron transfer occurs. Low quantum yield electron photodetachment from ferrioxalate has also been observed.

1. Introduction

The ferrioxalate complex is known to be photochemically active after excitation with ultraviolet and visible light[1] and undergoes the accepted overall reaction 1.1:[2]

$$2[Fe(III)(C_2O_4)_3]^{3-} + h\nu \rightarrow 2[Fe(II)(C_2O_4)_2]^{2-} + C_2O_4 + 2CO_2\uparrow \quad (1.1)$$

The absorption spectrum of $[Fe(III)(C_2O_4)_3]^{3-}$ in water consists of two broad bands. One has its maximum at 210 nm ($\varepsilon = 1.2 \times 10^4$ cm^{-1} M^{-1}) and the other at 669 nm ($\varepsilon =$ 0.94 cm^{-1} M^{-1}). The intense absorption at 210 nm has been attributed to the charge transfer (CT) band,[3] while the weak 669 nm band has been assigned to a d−d spin forbidden transition.[4] The Fe(III) to Fe(II) ferrioxalate photoredox reaction and its quantum yield have been studied in detail within the 254–505 nm range by Parker et al.,[1] who first suggested the use of ferrioxalate as a sensitive chemical actinometer. The quantum yield for the Fe(II) formation after excitation at wavelengths between 254 and 405 nm has been found to be larger than one and be independent of excitation energy; however, it decreases toward zero at longer wavelengths.[1] A tentative explanation provided by Porter et al.[3] was that, at the longer wavelengths, primary recombination or the competition with collisional deactivation may decrease the quantum yield. The excitation energy dependence has also been observed in ^{13}C isotope experiments,[5] where this effect is present in the 366–520 nm range but not at wavelengths shorter than 366 nm. Those experimental results point out that although the ferrioxalate molecule is photosensitive in a wide excitation energy range, the photoredox mechanisms might be different.

Various methods, especially transient spectroscopic studies, have been applied to the study of the photoreaction of ferrioxalate in order to interpret its photoredox mechanisms.[2,6–10] A preliminary flash photolysis study was performed by Parker et al. in 1959,[2] who proposed that intramolecular electron transfer (ET) was the primary reaction after excitation. More detailed kinetic studies by Cooper et al. in 1971 using 340–500 nm irradiation[6] suggested that the dissociation of ferrioxalate without intramolecular ET must be also considered as a possible primary process. Laser photolysis at 347 nm was employed by Nadtochenko et al. in 1996 to study the fast kinetics of ferrioxalate and its interaction with toxic pollutants such as phenol.[9] Lately,

* To whom correspondence should be addressed. E-mail: pmrentze@uci.edu.

(1) Parker, C. A. *Proc. R. Soc. London, Ser. A.* **1953**, *220*(1140), 104–116.
(2) Parker, C. A.; Hatchard, C. G. *J. Phys. Chem.* **1959**, *63*(1), 22–26.
(3) Porter, G. B.; Doering, J. G. W.; Karanka, S. *J. Am. Chem. Soc.* **1962**, *84*, 4027.
(4) Balzani, V.; Carassiti, V. *Photochemistry of Coordination Compounds*; Academic Press Inc.: New York, **1970**.
(5) Betts, R. H.; Buchannon, W. D. *Can. J. Chem.* **1976**, *54*(16), 2577–2580.
(6) Cooper, G. D.; DeGraff, B. A. *J. Phys. Chem.* **1971**, *75*(19), 2897.
(7) Patterso, Ji.; Perone, S. P. *J. Phys. Chem.* **1973**, *77*(20), 2437–2440.
(8) Zipin, H.; Speiser, S. *Chem. Phys. Lett.* **1975**, *31*(1), 102–103.
(9) Nadtochenko, V.; Kiwi, J. *J. Photochem. Photobiol., A* **1996**, *99*, 145–153.

10.1021/ic7016566 CCC: $40.75
Published on Web 02/20/2008

time-resolved optical spectroscopic and time-resolved extended X-ray absorption fine structure (EXAFS)[11,12] studies have also been carried out using 400 nm excitation for the femtosecond (fs) to picosecond (ps) range and 355 nm for the nanosecond (ns) to millisecond (ms) time region.[10,13] These EXAFS data provided strong evidence for the support of a mechanism that involves ferrioxalate photodissociation before intramolecular ET. However, these studies provided kinetic and structural information that were limited to low excited states (400 nm), which might not belong to the CT band. Because of the structure of the absorption band and the low extinction coefficient at 400 nm, it was possible that the mechanism proposed for these lower excited levels may not necessarily apply to higher levels where the higher extinction coefficient CT band is located. In order to examine the possible photochemistry that may be initiated at energies located near the 210 nm maximum absorption wavelength of the CT band, we performed experiments with 266/267 nm pulses and considered the following reaction paths:

(1) Intramolecular ET: Proposed by Parker et al.,[2] intramolecular ET involves the decrease of the iron oxidation state due to one electron transfer from oxalate to iron.

$$[Fe(III)(C_2O_4)_3]^{3-} \xrightarrow{h\nu} [Fe(III)(C_2O_4)_3]^{3-} \rightarrow$$

$$[(\bullet C_2O_4)Fe(II)(C_2O_4)_2]^{3-} \rightarrow [Fe(II)(C_2O_4)_2]^{2-} + C_2O_4\bullet^-/CO_2, CO_2\bullet^- \quad (1.2)$$

This photoinduced reduction may generate the following molecular structure changes. First, for iron complexes with the same ligand, the Fe(II)−O bond length of Fe(II) complexes is usually 0.1–0.2 Å longer than the Fe(III)−O bond length of Fe(III) complexes.[13,14] Second, the relocalization/redistribution of one electron between the ligand and the metal will break down the D_3 symmetry of the original ferrioxalate molecule.

(2) Electron photodetachment: Photoelectron detachment has been known to occur in several Fe complexes, for example $[Fe(II)(CN)_6]^{4-}$.[15] Although direct photoionization of ferrioxalate in water with excitation lower than 4.7 eV is not expected, we have considered the possibility of the photodetachment of one electron from the ferrioxalate by the electrostatic attraction of the solvent to form solvated electrons.

$$[Fe(III)(C_2O_4)_3]^{3-} \xrightarrow{h\nu} [Fe(III)(C_2O_4)_3]^{3-} \rightarrow$$

$$[Fe(C_2O_4)_3]^{2-} + e_{aq}^- \quad (1.3)$$

During the electron detachment process, the electrostatic interaction between the ferrioxalate and the surrounding solvent molecules will change and the polarization of the ferrioxalate anion will increase due to the inhomogeneous interaction, which is expected to lead to modification of the Fe−O bond length.

(3) Photodissociation of Fe−oxalate: This mechanism involves the breakage of an Fe−O bond without electron transfer from the oxalate to iron; therefore, the oxidation state of iron remains at + 3.

$$[Fe(III)(C_2O_4)_3]^{3-} \xrightarrow{h\nu} [Fe(III)(C_2O_4)_3]^{3-} \rightarrow$$

$$[Fe(III)(C_2O_4)_2]^- + 2CO_2\bullet^- \quad (1.4)$$

This reaction mechanism will be shown to be the primary photochemical process that is responsible for the Fe−O bond distances becoming shorter by 0.06–0.10 Å after dissociation.

(4) Photoinduced spin crossover: Intersystem crossing between the low- and the high-spin electronic configurations has been observed in many six-coordinate metal complexes.[16,17] A metal–ligand bond length change of about 0.2 Å has been observed by picosecond EXAFS after photoinduced Fe(II) spin crossover.[18,19] For spin crossover of the Fe(III) complex, the molecule is first excited from its ground state (^{6}GS) to an upper electronic state with the same spin (^{6}ES), followed by intersystem crossing to a lower, ^{4}ES or ^{2}ES, spin state.

$$[Fe(III)(C_2O_4)_3]^{3-} (s = {}^5/_2) \xrightarrow{h\nu} [Fe(III)(C_2O_4)_3]^{3-} (s = {}^5/_2) \rightarrow$$

$$[Fe(III)(C_2O_4)_3]^{3-} (s = {}^3/_2, {}^1/_2) \quad (1.5)$$

These spin changes could be reflected by the structural modification of the ferrioxalate molecule and the difference absorption, ΔA.

According to mechanisms 1.2 and 1.3, the primary process after excitation involves electron transfer, either from the oxalate to the iron or from the ferrioxalate to the solvent. Mechanism 1.2 involves the direct reduction of Fe(III) to Fe(II). Mechanism 1.3 includes the solvated electron formed that may reduce Fe(III) to Fe(II) by a secondary reaction. Mechanism 1.4 and 1.5 do not involve electron transfer in the primary reaction step; therefore, the formation of the Fe(II) complex has to rely on other reductive species that are formed during the initial primary reaction such as carbon dioxide anion radical.[13] Although the reaction paths vary, they all lead to the structural rearrangements of transients that could only be substantiated by time-resolved X-ray spectroscopy,[20,21] especially by time-resolved EXAFS[11,12]

(10) Chen, J.; Zhang, H.; Tomov, I. V.; Ding, X. L.; Rentzepis, P. M. *Chem. Phys. Lett.* **2007**, *437*, 50–55.
(11) Bressler, C.; Chergui, M. *Chem. Rev.* **2004**, *104*, 1781–1812.
(12) Chen, L. X. *Annu. Rev. Phys. Chem.* **2005**, *56*, 221–254.
(13) Chen, J.; Zhang, H.; Tomov, I. V.; Wolfsberg, M.; Ding, X.; Rentzepis, P. M. *J. Phys. Chem. A* **2007**, *111*(38), 9326–9335.
(14) Kennepohl, P.; Solomon, E. I. *Inorg. Chem.* **2003**, *42*(3), 696.
(15) Rentzepis, P. M.; Jones, R. P.; Jortner, J. *Chem. Phys. Lett.* **1972**, *15*(4), 480.
(16) Brady, C.; McGarvey, J. J.; McCusker, J. K.; Toftlund, H.; Hendrickson, D. N. *Spin Crossover Transition Metal Compd. III* **2004**, *235*, 1–22.
(17) Gawelda, W.; Pham, V. T.; Benfatto, M.; Zaushitsyn, Y.; Kaiser, M.; Grolimund, D.; Johnson, S. L.; Abela, R.; Hauser, A.; Bressler, C.; Chergui, M. *Phys. Rev. Lett.* **2007**, *98*(5), 057401.
(18) Khalil, M.; Marcus, M. A.; Smeigh, A. L.; McCusker, J. K.; Chong, H. H. W.; Schoenlein, R. W. *J. Phys. Chem. A* **2006**, *110*, 38–44.
(19) Pandey, R. K.; Mukamel, S. *J. Phys. Chem. A* **2007**, *111*(5), 805–816.
(20) Pfeifer, T.; Spielmann, C.; Gerber, G. *Rep. Prog. Phys.* **2006**, *69*(2), 443–505.
(21) Gaffney, K. J.; Chapman, H. N. *Science* **2007**, *316*(5830), 1444–1448.

and possibly excited-state structure calculations such as TurboMol.[22] In this article, the time-resolved kinetics and structural changes induced by short wavelength excitation are investigated by means of femtosecond to millisecond transient optical and ultrafast EXAFS studies using 266/267 nm pulsed excitations and 0.6 ps hard X-ray pulse continuum to monitor changes in structure as a function of time (picoseconds). In addition, we have performed density functional theory (DFT; B3LYP/6-31G) quantum chemical and Hartree–Fock (UHF/6-31G) calculations that provide strong supporting evidence that has helped us to elucidate the mechanism of the photoredox reaction of ferrioxalate in aqueous solution. The experimental results observed previously[10,13] with 355/400 nm excitations are also considered here and compared with the 266/267 nm data obtained in this study.

2. Experiments and Results

2.1. Kinetics of Ferrioxalate Photoredox Reaction. $(NH_4)_3Fe(III)(ox)_3 \cdot 3H_2O$, where ox = $C_2O_4^{2-}$, purchased from Alfa Aesar was dissolved in distilled water. The ferrioxalate photoredox reaction experiments presented in this article were conducted at room temperature using 266 nm pulses for picosecond to millisecond and 267 nm for the femtosecond to picosecond range. The absorption extinction coefficient of ferrioxalate was determined to be 4.8×10^3 cm^{-1} M^{-1} at 266 and 267 nm, which is close to the literature value.[1] When the concentrations of ferrioxalate water solution were higher than 1 mM, the effect of oxygen was neglected.[23] The three laser systems that were used to study the photochemical kinetics of ferrioxalate from femtoseconds to milliseconds have been described previously.[10,13] In the present studies, we used 100 fs, 0.3 mJ, and 267 nm pulses generated by the Ti:sapphire third harmonic, as the pump pulse for the femtosecond to picosecond experiments and 266 nm pulses (fourth harmonic of the Nd:YAG) for picosecond to millisecond experiments. The concentrations for the time-resolved transient optical measurements were 1.6 and 2.3 mM for the femtosecond to nanosecond and nanosecond to millisecond ranges, respectively. Our transient optical data show that after excitation with 266/267 nm femtosecond to nanosecond pulses, two fast transient absorption bands were formed at 500–800 and 380–500 nm, respectively. Figures 1−3 show the time-resolved spectra of the femtosecond/picosecond, picosecond/nanosecond, and nanosecond/microsecond experiments respectively.

(1) 500–800 nm band: The 500–800 nm transient band is formed immediately after 267 nm femtosecond excitation, and its maximum wavelength appears to red shifts continuously from 570 to 720 nm as shown in Figure 1 owing to dispersion. The femtosecond kinetic data are plotted in Figure 4 as ΔOD (OD = optical density) at 720 nm vs delay time, and the insert shows that the photolysis is a single-photon process. This transient band has also been observed previously with 400 nm excitation, except that it was formed by a two-photon process. These absorption bands formed by 267 and 400 nm excitation are found to be practically identical in shape, width, and spectral range; therefore, we

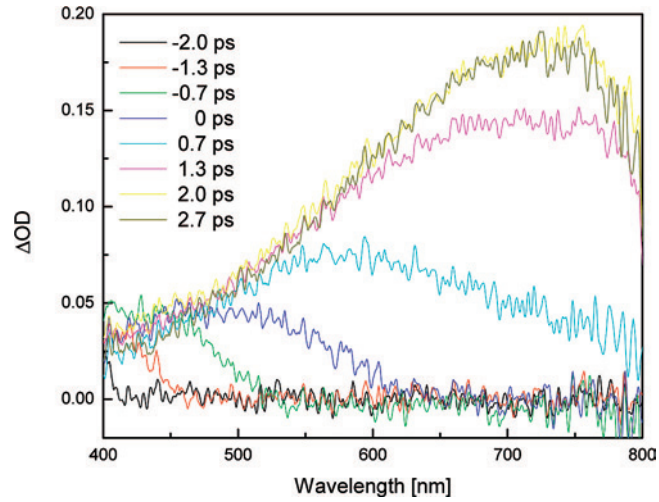

Figure 1. Femtosecond time-resolved transient absorption spectra of 1.6×10^{-3} M ferrioxalate in water (267 nm excitation).

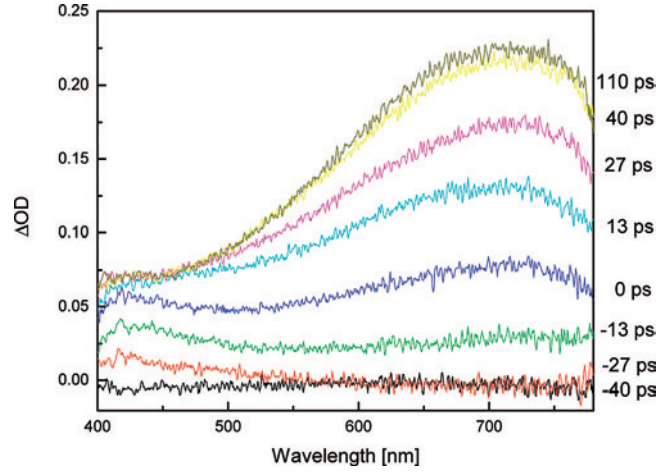

Figure 2. Picosecond time-resolved transient absorption spectra of 1.6×10^{-3} M ferrioxalate in water (266 nm excitation).

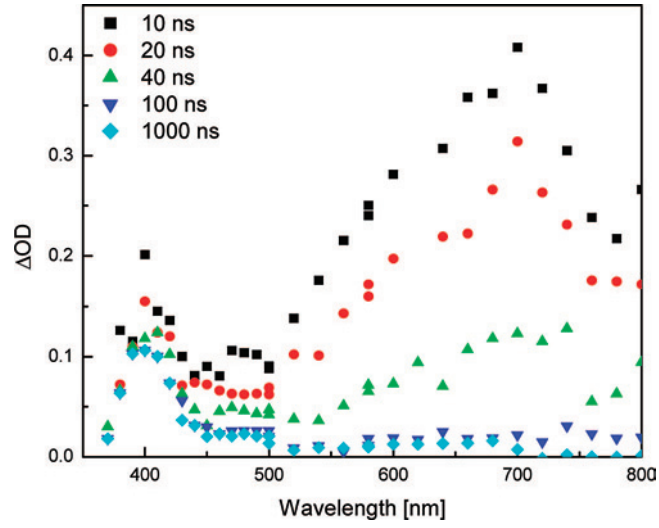

Figure 3. Nanosecond transient absorption spectra of 2.3×10^{-3} M ferrioxalate in water (266 nm excitation).

(22) Ahlrichs, R.; Bar, M.; Haser, M.; Horn, H.; Kolmel, C. *Chem. Phys. Lett.* **1989**, *162*(3), 165–169.
(23) Jeong, J. S.; Yoon, J. Y. *Water Res.* **2004**, *38*(16), 3531–3540.

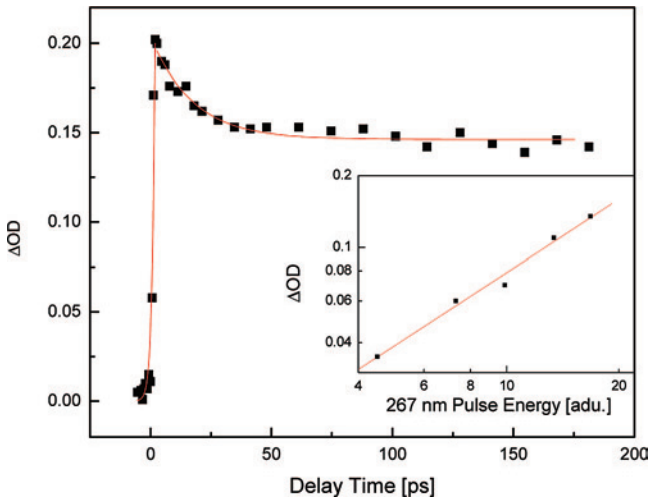

Figure 4. Kinetics of the 720 nm transient absorption band of 1.6×10^{-3} M ferrioxalate in water excited with 267nm laser pulse. (inset) 720 nm transient absorption intensity vs excitation energy (slope = 1.0).

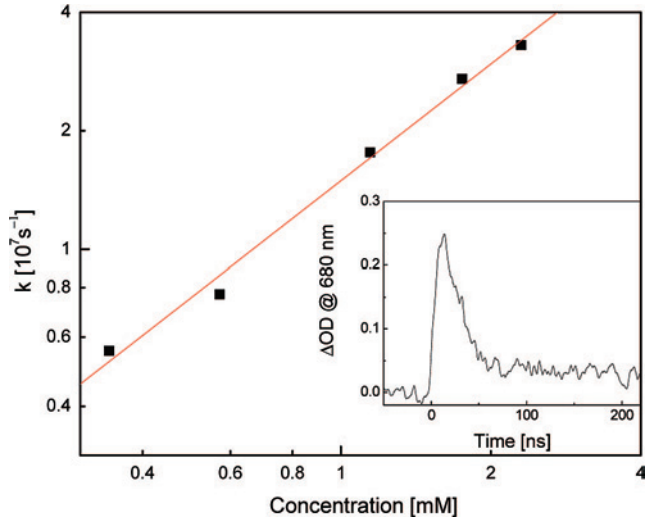

Figure 5. Nanosecond decay rate constant of the 680 nm transient absorption band vs concentration of ferrioxalate (slope = 0.99). (inset) Nanosecond kinetics of 2.3×10^{-3} M ferrioxalate in water (266 nm excitation).

assign them to the same intermediate(s). A very similar 500–800 nm band had been detected also after picosecond/nanosecond and nanosecond/microsecond 266 nm excitation with apparent formation times of about 45 ps and less than 10 ns, respectively. Both of these formation times are artificial because they are due to the width of the excitation pulses with the true formation time having been determined in the femtosecond to picosecond experiments to be 1.3 ps. The shape of these bands, see Figures 2 and 3, are similar to the 500–800 nm band observed in the femtosecond/picosecond experiments; therefore, we attribute the 4 ps to 10 ns 500–800 nm transient bands to the same intermediate whose assignment we shall discuss later. After the 500–800 nm band reaches its maximum absorbance at about 2 ps, it is followed by a two-component decay with the short-lived component having a decay lifetime of 17 ps as shown in Figure 4. The long component decay kinetics shown in Figure 5 were found to decay with lifetimes of 30 ns at 2.3 mM and 130 ns at

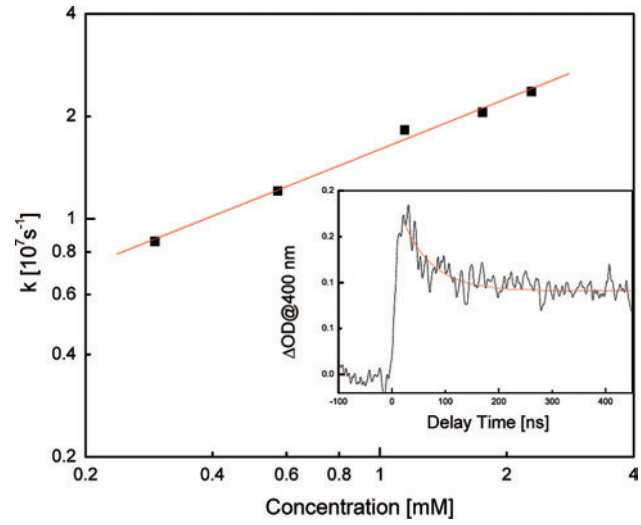

Figure 6. Nanosecond decay rate constant of the 400 nm transient absorption band vs concentration of ferrioxalate (slope = 0.49). (inset) Nanosecond kinetics of 1.1×10^{-3} M ferrioxalate in water (266 nm excitation).

0.57 mM. All of these experiments were performed with nitrogen bubbling in order to minimize the effect of oxygen on the decay of this transient band.

(2) 380–500 nm band: The 380–500 nm band with maximum absorption at 410 nm is formed immediately after excitation with 6 ns, 266 nm pulses. This band, shown in Figure 3, is similar to the transient absorption band that was detected by us after 355 nm excitation[13] and by Nadtochenko and Kiwi 100 ns after 347 nm excitation.[9] A similar 400–500 nm transient band that overlaps with the tail of the 500–800 nm transient band is also observed using 266 nm femtosecond and 267 nm picosecond pulse excitations as shown in Figures 1 and 2. Our time-resolved studies indicate that the nanosecond transient absorption band located at 400 nm has a two-component decay. The short-lived component was found to be concentration dependent decaying with a lifetime of 42 ns at 2.3 mM (see Figure 6), and the long-lived component decays with a lifetime of 0.49 ms at 2.3 mM.

2.2. Ultrafast EXAFS. The picosecond time-resolved EXAFS experiments were performed using a tabletop laser pulsed ultrashort X-ray source system, which generates both 100 fs, 267 nm pump pulses and 0.6 ps X-ray continuum pulses that were used to probe the structure of the intermediates formed after excitation.[10,13,24] The concentration used for time-resolved EXAFS experiments was 1.0 M, which corresponds to $\mu x \sim 0.6$ (μ = X-ray mass absorption coefficient, x = length of X-rays path through the sample) for 7.1 keV radiation. It was estimated that for the EXAFS experiments each 267 nm pulse excites about 10% of the ferrioxalate molecules in its path; therefore, the amount of Fe(II) product formed was negligible compared to the 100 mL total volume used. Precise spatial and temporal overlap of the 267 nm optical pump beam and the 6.5–8.5 keV X-ray probe beam, which is mandatory for accurate data, was achieved using the previously published procedure described

(24) Tomov, I. V.; Chen, J.; Ding, X.; Rentzepis, P. M. *Chem. Phys. Lett.* **2004**, *389*(4–6), 363–366.

in refs 10 and 13. To optimize the X-ray flux, we utilized an X-ray lens which could focus X-rays onto the sample and positioned such that the short focal length faced the source and the long focal length faced the sample solution.[13,24] The sample to crystal and crystal to CCD distances were 120 and 100 mm respectively. In this configuration, the energy resolution was estimated to be 20 eV, which is limited mostly by the size of X-ray lens focal spot and the distance between the X-ray lens focal spot and the detector. A typical EXAFS spectrum at a particular delay time was achieved by adding together 25 1-h EXAFS spectra. The characteristic tungsten L lines are used for energy calibration. The tungsten L_l line which is located at 7.39 keV is responsible for the large noise in the data collected in the 7.25–7.35 keV range. One of the possible solutions would be change the X-ray source from tungsten to other metals, such as molybdenum. However, we found that the continuum output intensity from molybdenum is not high enough to perform EXAFS with an acceptable signal to noise ratio (S/N).

The EXAFS data analysis was performed with a standard automated data reduction program, ATHENA[25] and an ab initio multiple scattering calculation program for EXAFS and XANES(X-ray absorption near edge structure) spectra, FEFF 8.20.[26] The EXAFS spectrum of the X-rays passing through air only was used as the background spectrum for subtraction. Here, k^2-weighted EXAFS spectra, where $k = (2m(E - E_o)/\hbar^2)^{1/2}$ (m is the mass of an electron, $E_0 = 7131$ eV), are Fourier transformed over the 2–7.5 $Å^{-1}$ range using a Kaiser−Bessel window. The EXAFS spectra were collected between 6.5 and 8.5 keV, which is determined by the divergence of the X-ray lens and the size of the CCD detector. However, only 7.05–7.35 keV ($k = 2$–7.5 $Å^{-1}$) was used for data analysis. The lower and upper limits are determined by the Fe K-edge (7.13 keV) and tungsten L_l line (7.39 keV, $k = 8.2$ $Å^{-1}$). The fit of our experimental spectra with the calculated EXAFS spectra by FEFF 8.20 was not very good because there was (1) a low S/N owing to the low X-ray flux and (2) a short k range that is limited by the tungsten L_l line. Therefore, we extracted the Fe−O bond length from the EXAFS μx vs energy spectra, Figure 7, and used the path of the first Fe−O shell for phase correction, which is calculated using FEFF 8.20 based on the crystalline structure of $[Fe(III)(C_2O_4)_3]^{3-}$.[27] Finally, the Fe−O bond length is represented as a $|\chi(R)|$ vs R spectra, Figure 8, which exhibits the bond distance between iron and oxygen of the first coordination shell. In this paper, we are concerned only with EXAFS and do not analyze XANES spectra which is the subject of another study. Using our time-resolved EXAFS experimental system, we determined that the Fe(III)−O bond distance of the parent molecule, 20 ps before excitation, is 1.99 Å, which is in good agreement with the 2.00 Å literature value of the Fe(III)−O bond distance

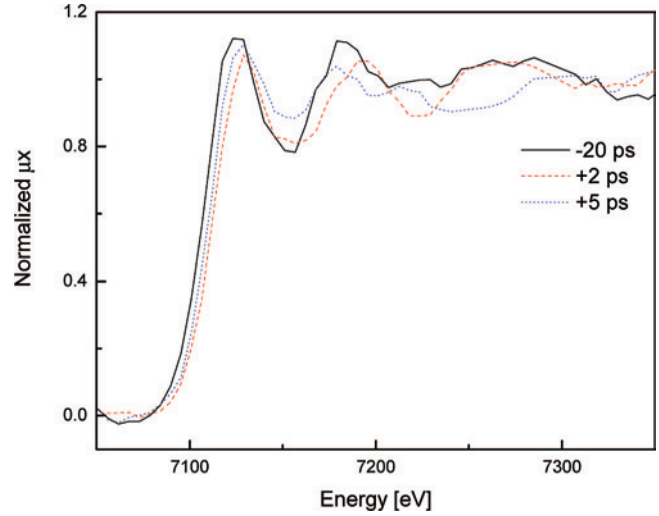

Figure 7. EXAFS spectra plotted as normalized μx vs energy at −20 ps before 267 nm excitation(solid line), +2 ps (dashed line), and +5 ps (dotted line) after 267 nm excitation.

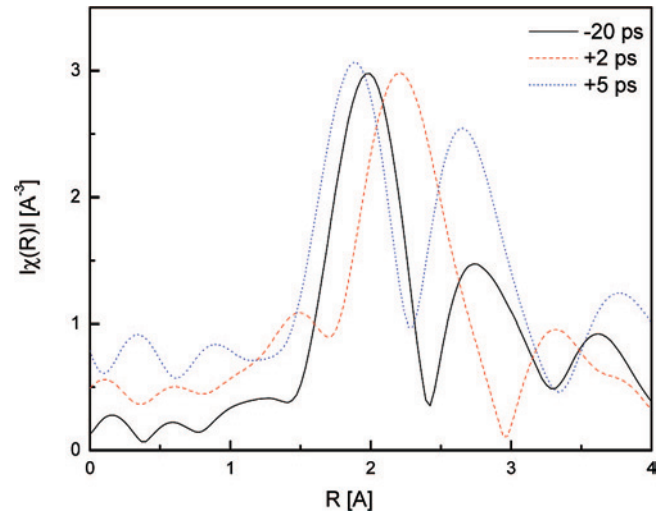

Figure 8. R space EXAFS spectra of ferrioxalate/water solution before (solid line, −20 ps) and after (dashed line, +2 ps and dotted line, +5 ps) 267 nm UV radiation.

for crystalline $[Fe(III)(C_2O_4)_3]^{3-}$.[27] Our previous time-resolved Fe−O bond length measured also at 20 ps before 400 nm excitation was 2.02 Å,[13] while the value obtained with a normal X-ray tube was 1.98 Å and the DFT calculations yield a value of 2.01 Å. The time and spatial resolution of this ultrafast X-ray system is estimated to be 2 ps and 0.04 Å, respectively.[13] The changes of the Fe−O bond length observed as a function of time during the first 140 ps are summarized in Table 1.

Full geometry optimizations were performed for the ground-state of each assigned structure by ab initio UHF and DFT calculations using the Gaussian 03 code.[28] The basis set 6-31G was employed for all ground-state calculations. The Becke three-parameter hydride functional with the Lee–Yang–Parr correlation corrections (B3LYP) was used in the DFT calculations. Some of the theoretical results have

(25) Ravel, B.; Newville, M. *J. Synchro. Rad.* **2005**, *12*, 537–541.
(26) Ankudinov, A. L.; Bouldin, C. E.; Rehr, J. J.; Sims, J.; Hung, H. *Phys. Rev. B* **2002**, *65*, 104107.
(27) Merrachi, E. H.; Mentzen, B. F.; Chassagneus, F.; Bouix, J. *Rev. Chim. Miner.* **1987**, *24*, 56–67.
(28) Frisch, M. J., et al. *Gaussian 03*, revision C.02; Gaussian, Inc.: Wallingford, CT, 2004.

Table 1. Fe−O bond length obtained by time-resolved EXAFS and quantum chemistry calculations at various delay time before and after 267 or 400 nm excitation

			exp R(Å)		cal R(Å)	
delay time	assignment	ligand	267 nm excitation	400 nm excitation	UHF	DFT
−20 ps	$[Fe(III)(C_2O_4)]^{3-}$	C_2O_4	1.99	2.02	2.04	2.01
0–2 ps	$[Fe(C_2O_4)_3]^{3-*}$	C_2O_4	2.21	2.16	N/A	N/A
4 ps	$[Fe(III)(\kappa^1 - C_2O_4)(\kappa^2 - C_2O_4)_2]^{3-}$	$\kappa^1 - C_2O_4$			1.87	1.87
		$\kappa^2 - C_2O_4$	1.92	1.93–2.09	2.01	2.02
5–140 ps	$[Fe(III)(C_2O_4)_2]^-$tetrahedral-like	C_2O_4	1.89–1.93	1.87–1.93	1.90	1.90
110 ns−2 ms	$[Fe(II)(C_2O_4)_3]^{4-}$	C_2O_4	N/A	N/A	N/A	N/A
	$[Fe(II)(C_2O_4)_2]^{2-}$tetrahedral-like				2.04	2.01

been reported previously,[10,13] and the very good agreement found between theoretical and experiment data has made it possible to interpret the 400 nm excitation experiments with confidence. The results of ground-state structure calculations and the assigned iron oxalate complexes are summarized in Table 1. The calculation of $[Fe(III)(C_2O_4)_3]^{3-}$ ion structure started with the published crystal structure without further symmetry restrictions. The $[Fe(III)(C_2O_4)_3]^{3-}$ ion was found to have an approximate D_3 symmetry with an accuracy of 0.003 Å while the symmetries of $[Fe(III)(C_2O_4)_2]^-$ and $[Fe(II)(C_2O_4)_2]^{2-}$ were both determined to be D_{2d}.

3. Discussions

3.1. Photoelectron Detachment and Solvated Electron. The 500–800 nm transient absorption band with λ_{max} at ∼720 nm that was observed after 266/267 nm excitation is very similar to the well-known spectrum of solvated electrons in water,[29,30] which has a broad, structureless absorption band with a maximum at ∼720 nm. The formation kinetics of this band determined in this study, Figure 4, are in agreement with the reported time-resolved formation kinetics for solvated electron.[29,30] To ascertain the formation of solvated electrons, we also performed electron quenching experiments using 0.1–0.2 M KNO_3, which has been used widely as an effective electron quencher.[31,32] The picosecond to nanosecond time-resolved solvated electron reaction data with and without KNO_3 are shown in Figure 9. The rate constant of the electron and K^+ cation reaction is small;[29] therefore, the effect of K^+ may be ignored when evaluating the electron scavenger/solvated electron reaction rate. The decay lifetime of the 500–800 nm band was determined to be longer than 3.7 ns without electron scavenger addition to the Fe(III)ox solution. However, the intensity of this band decreased significantly within 300 ps after nitrate was added to the solution. We also determined that the decay lifetime of the 500–800 nm band depends upon the concentration of the nitrate added to the solution, corresponding to 7.9×10^{-10} s at 0.1 M and 2.8×10^{-10} s at 0.2 M NO_3^-. The bimolecular quenching constants derived from these lifetimes are 1.3–1.8 $\times$ 10^{10} M^{-1} s^{-1}, which agree with the literature values reported for the solvated electron/nitrate reaction.[31,32] The good agreement of both spectra and quenching constants with the previously published results[29–32] strongly suggests that the observed absorption band at 500–800 nm is due to solvated electrons.[33]

In our experiments, the solvated electrons were generated by 267 nm, 4.64 eV pulses by inducing photoelectron detachment from the ferrioxalate anion and its subsequent transfer to solvent. Charge transfer to solvent (CTTS) theoretical and experimental studies have been reported for a long period of time,[34] and several of these studies have been applied specifically to ferrocyanide and other metal–ligand systems.[30,35] Even though, to our knowledge, the ionization potential of ferrioxalate in solution is not known, the ionization potential of the Fe atom is known to be I_P = 7.87 eV.[36] Photoelectron spectroscopy studies on hydrated electron cluster anions have determined that the photoelectric threshold is ∼3.25 eV for the hydrated electron in bulk water solution, which corresponds to the solvation energy of electrons in water.[37] The difference of 4.62 eV between these two values is the minimum energy necessary to excite the ferrioxalate molecule to the CTTS state and induce electron photodetachment. Using these values, we see that it is possible for one 267 nm photon, 4.64 eV, to populate the ferrioxalate molecule to the 4.62 eV metastable CTTS state, which subsequently yields a detached electron. In view of these values, it also becomes evident why the 400 nm, 3.10 eV, pulse may not excite the molecule to the CTTS state by one photon, but only by a two-photon process.[10,13]

The solvated electron, which is known to have a high redox potential (E^0 = approx. −2.7 V(NHE)),[38] may react with the parent ferrioxalate and reduce Fe(III) to Fe(II) according to reaction 3.2. Assuming this 500–800 nm band is due to solvated electrons, the reaction constant of the solvated electron and ferrioxalate reaction derived from the decay lifetime of this band is estimated to be 1.5×10^{10} M^{-1} s^{-1}. This value agrees with

(29) Baxendale, J. H.; Capellos, C.; Land, E. J.; Keene, J. P.; Ebert, M.; Swallow, A. J.; Davies, J. V.; Francis, J. M.; Gilbert, C. W.; Fielden, E. M.; Nosworthy, J. M. *Nature* **1964**, *201*(491), 468.
(30) Pommeret, S.; Naskrecki, R.; van der Meulen, P.; Menard, M.; Vigneron, G.; Gustavsson, T. *Chem. Phys. Lett.* **1998**, *288*(5–6), 833–840.
(31) Jonah, C. D.; Miller, J. R.; Hart, E. J.; Matheson, M. S. *J. Phys. Chem.* **1975**, *79*(25), 2705–2711.
(32) Wiesenfeld, J. M.; Ippen, E. P. *Chem. Phys. Lett.* **1980**, *73*(1), 47–50.
(33) Zhang, H.; Chen, J.; Tomov, I. V.; Dvornikov, A. S.; Rentzepis, P. M. *J. Phys. Chem. A* **2007**, *111*(45), 11584–11588.
(34) Blandame, M. j. *Chem. Rev.* **1970**, *70*(1), 59.
(35) Sauer, M. C.; Crowell, R. A.; Shkrob, I. A. *J. Phys. Chem. A* **2004**, *108*(25), 5490–5502.
(36) Schildcr, S. M.; Pearson, R. G.; Stafford, F. E. *J. Am. Chem. Soc.* **1968**, *90*(15), 4006.
(37) Coe, J. V.; Lee, G. H.; Eaton, J. G.; Arnold, S. T.; Sarkas, H. W.; Bowen, K. H.; Ludewigt, C.; Haberland, H.; Worsnop, D. R. *J. Chem. Phys.* **1990**, *92*(6), 3980–3982.
(38) Schwarz, H. A.; Dodson, R. W. *J. Phys. Chem.* **1989**, *93*(1), 409–414.
(39) Crowell, R. A.; Lian, R.; Shkrob, I. A.; Bartels, D. M.; Chen, X. Y.; Bradforth, S. E. *J. Chem. Phys.* **2004**, *120*(24), 11712–11725.

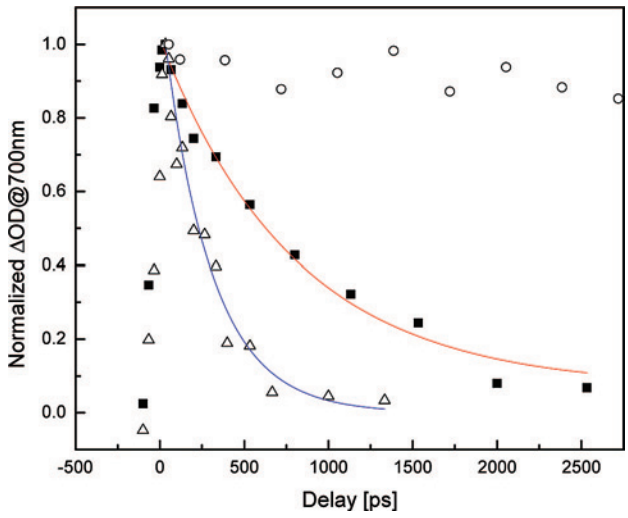

Figure 9. Picosecond kinetics of the 700 nm transient absorption band of 3.3×10^{-3} M ferrioxalate in water at various KNO_3concentrations: (circle) 0, (square) 0.1, and (triangle) 0.2 M.

the 1.2×10^{10} M^{-1} s^{-1} rate constant of the electron and cobaltoxalate reaction reported in ref 29.

The kinetic scheme of this reaction path is summarized as:

$$[Fe(III)(C_2O_4)_3]^{3-} \overset{h\nu}{\leftrightarrow} [Fe(C_2O_4)_3]^{2-} + e_{aq}^- \quad (3.1)$$

$$e_{aq}^- + [Fe(III)(C_2O_4)_3]^{3-} \rightarrow [Fe(II)(C_2O_4)_3]^{4-} \quad k = 1.5 \times 10^{10}\ M^{-1}\ s^{-1} \quad (3.2)$$

We proposed that the photoelectron detached from the $Fe(III)(C_2O_4)_3]^{3-}$ anion is located primarily on the oxalate group and forms the $[Fe(C_2O_4)_3]^{2-}$ complex following reaction 3.1. According to our calculations, the Fe−O bond distance in the $[Fe(C_2O_4)_3]^{2-}$ complex is about 0.2 Å longer than that in the original $[Fe(III)(C_2O_4)_3]^{3-}$ complex. However, those changes in the structure have only a small effect on the measured Fe−O bond distance change due to the relative low quantum yield that is described in some detail below. Figure 4 shows the fast decay of the solvated electron band with a lifetime of 17 ps, which we assign to the cage recombination of the photodetached electron with the $[Fe(C_2O_4)_3]^{2-}$ complex according to the back reaction 3.1. Such fast solvated electron recombination has been reported previously[39,40] listing a decay lifetime of 13 ps. We find that the 500–800 nm solvated electron band does not decay to zero but reaches a plateau at ΔOD = 0.14, which suggested that only 30% $[Fe(C_2O_4)_3]^{2-}$ reacts with electrons via cage geminate recombination. $[Fe(C_2O_4)_3]^{2-}$ may also diffuse out the solvation cage and react with a solvated electron to form ferrioxalate or dissociate to $CO_2\bullet^-$or $C_2O_4\bullet^-$as shown in reactions 3.3 and 3.4, respectively. However, those reaction paths are difficult to distinguish.

$$[Fe(C_2O_4)_3]^{2-} + e_{aq}^- \rightarrow [Fe(III)(C_2O_4)_3]^{3-} \quad (3.3)$$

$$[Fe(C_2O_4)_3]^{2-} \rightarrow [Fe(III)(C_2O_4)_2]^- + C_2O_4\bullet^-/CO_2\bullet^-, CO_2 \quad (3.4)$$

3.2. Dissociation and Intermolecular Electron Transfer. The 400–500 nm transient has been observed previously[10,13] with 355/400 nm excitation, and experimental evidence has indicated that dissociation instead of intramolecular electron transfer is probably the primary process. We do not however exclude intermolecular ET completely. The postulated mechanism for the Fe(III) to Fe(II) reduction reaction, where dissociation is found to precede intramolecular electron transfer is outlined as follows:

$$[Fe(III)(C_2O_4)_3]^{3-} \xrightarrow{h\nu} [Fe(III)(C_2O_4)_3]^{3-} \quad (3.5)$$

$$[Fe(C_2O_4)_3]^{3-} \rightarrow [Fe(III)(\kappa^1 - C_2O_4)(\kappa^2 - C_2O_4)_2]^{3-} \rightarrow [Fe(III)(C_2O_4)_2]^- + 2CO_2\bullet^- \quad (3.6)$$

$$[Fe(III)(C_2O_4)_2]^- + CO_2\bullet^- \rightarrow [Fe(II)(C_2O_4)_2]^{2-} + CO_2\uparrow \quad k = 4.0 \times 10^9\ M^{-1}\ s^{-1} \quad (3.7)$$

$$[Fe(III)(C_2O_4)_3]^{3-} + CO_2\bullet^- \rightarrow [Fe(II)(C_2O_4)_3]^{4-} + CO_2\uparrow \quad k = 4.0 \times 10^9\ M^{-1}\ s^{-1} \quad (3.8)$$

On the basis of the ultrafast EXAFS data obtained with 267 nm excitation, we determined that the Fe−O bond length has a value of 1.99 Å, in the original nonirradiated molecule, which increases to 2.21 Å during the first 2 ps after excitation and then to 1.89–1.92 Å after 4 ps. Subsequently, it remains constant at 1.93 Å for the 140 ps time span capability of our femtosecond EXAFS system. These bond length changes are similar to the values obtained with 400 nm excitation, which are 2.02 Å for the parent molecule, 2.16 Å at +2 ps, 1.93 Å after 4 ps, and 1.87 Å for 5–115 ps. On the basis of the similarity of the 400–500 nm transient absorption bands and the Fe−O bond length changes obtained using 267 and 400 nm excitations, we conclude that after 267 nm photoexcitation the ferrioxalate molecule follows the same reaction path described by reactions 3.5−3.8, and we attribute the structural changes observed to the following transient species:

(1) 0–2 ps, excited state: The Fe−O bond length measured at 2 ps after 267 nm excitation by our ultrafast EXAFS system was 2.21 Å, which is very close to but longer than the 2.16 Å value obtained 2 ps after 400 nm excitation,[10] Table 1. This 2.21 Å Fe−O bond length is attributed to an excited-state ferrioxalate, $[Fe(III)(C_2O_4)_3]^{3-*}$, which has been elongated by 0.2 Å compared to the ground-state molecule. One of the possibilities is that the 267 nm excited state has a longer Fe−O bond length than the 400 nm excited state because of its higher excitation energy. On the basis of DFT and UHF calculations, both the LUMO and HOMO of the ground state are mixed orbitals with both Fe and oxalate ligand character. The Fe character in the LUMO is predicted to be larger than that in the HOMO, which suggests that partial charge transfer may take place immediately after excitation. The mixed character in LUMO suggests a

(40) Lian, R.; Oulianov, D. A.; Crowell, R. A.; Shkrob, I. A.; Chen, X. Y.; Bradforth, S. E. *J. Phys. Chem. A* **2006**, *110*(29), 9071–9078.

transition to an antibonding σ^* orbital where the Fe−O bond was weakened and therefore became longer in contrast to a possible $\pi-\pi^*$ transition where the Fe−O bond length is not expected to have large changes. We have performed calculations on the structure of the excited state using TD-DFT by Gaussian 03 and TurboMol; however, the results were not as reliable as DFT for the ground-state structure. The absence of excited-state structural information is another major obstacle in fitting the experimental EXAFS data besides the short k range and relative low S/N.

(2) 3–4 ps five-coordinated Fe(III) oxalate complex: The Fe−O bond lengths obtained using 267 nm excitation were measured to be 1.92 Å after 4 ps, which is close to the reported 1.93 Å Fe−O bond distance for $[Fe(III)(\kappa^1 - C_2O_4)(\kappa^2 - C_2O_4)_2]^{3-}$ five-coordinate complex,[10] which is proposed to be formed after breaking one Fe−O bond.

(3) 5–140 ps four-coordinated Fe(III) oxalate complex: The Fe−O bond distances obtained were determined to be 1.89 Å 5 ps after 267 nm excitation and then remain 1.93 Å for at least 140 ps. Both values are close to the 1.87 Å value measured by EXAFS for the same time after 400 nm excitation. This 1.89–1.93 Å Fe−O bond length is assigned to the $[Fe(III)(C_2O_4)_2]^-$ four-coordinated dissociation product.

In a previous study,[10] it was shown that the energy of one 400 nm photon, 3.10 eV, is sufficient to break two Fe−O bonds and one C−C bond. The reaction path after 267 nm excitation involves the population of an excited state, with a 2.21 Å Fe−O bond distance, followed by the dissociation of one Fe−O bond (1.92 Å) and then complete dissociation of one oxalate group (1.89–1.93 Å); see reaction 3.5. The similarity of the Fe−O bond length changes after excitation with either 400 or 267 nm femtosecond pulses (see Table 1) strongly suggests that the molecule follows the same reaction path for both the 400 and 267 nm excited states. We assigned the 1.92 and 1.89 Å transients to $[Fe(III)(\kappa^1 - C_2O_4)(\kappa^2 - C_2O_4)_2]^{3-}$ and $[Fe(III)(C_2O_4)_2]^-$, respectively. This assignment which is based on comparison with the data obtained with the 400 nm excitation femtosecond pulses indicates that the dissociation product $[Fe(III)(C_2O_4)_2]^-$ remains initially in the Fe(III) oxidation state and suggests that although the electron density of the excited LUMO orbital state of iron has increased, high yield intramolecular ET from oxalate to iron does not take place during the first 100 ps after excitation. One 267 nm photon excites the ferrioxalate molecule to a higher excited state than the 400 nm excited level, and both states are expected to be located above the dissociative potential; however, it is difficult to distinguish between predissociation and direct dissociation from the 267 nm excited level.

The structural changes that occur at times longer than 140 ps after excitation could not be measured by our present femtosecond X-ray system. However, transient optical spectroscopic data were obtained and are used to determine the reaction mechanism at times longer than 140 ps. After dissociation of one oxalate, the highly reactive $CO_2^{\bullet-}$ anion radical was generated by reaction 3.6, which could react with Fe(III) and reduce it to the Fe(II) complex by intermolecular ET following the paths of reactions 3.7 and 3.8. The decay

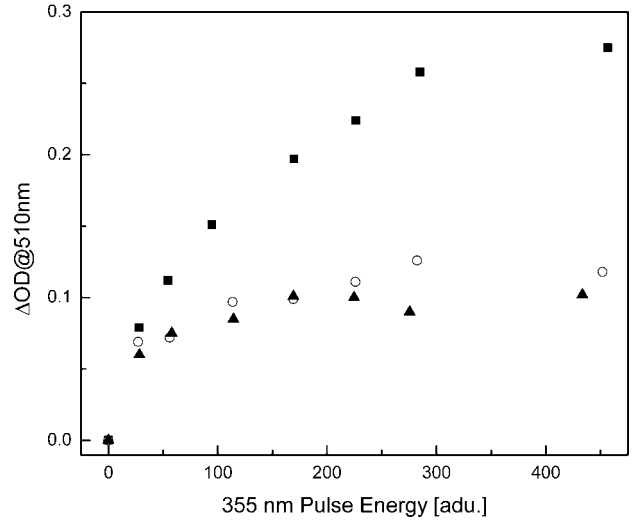

Figure 10. Optical density of $[Fe(II)(phen)_3]^{2+}$ complex at 510 nm plotted as a function of 355 nm pulse energy. The concentrations of thymine are represented by the following: (square) 0, (circle) 5×10^{-5}, and (triangle) 2.5×10^{-4} M.

rate constant of the 380–500 nm band measured using 266 nm excitation was found to increase when the concentration of ferrioxalate was increased. These experimental data support the conclusion that 266 nm excitation first leads to dissociation of ferrioxalate and then to intermolecular ET. To further investigate this conclusion, we performed radical scavenging experiments which allow us to determine the nature of the photodissociation species generated and make it possible to describe in detail the photochemical reactions and mechanism. Thymine is known to be an effective $CO_2^{\bullet-}$ anion radical scavenger.[10,41] Due to the strong absorption of thymine at 266 nm, we performed a series of $CO_2^{\bullet-}$ radical scavenging experiments using 355 nm pulse excitation, which is expected to initiate the same photochemistry as the 400 and 266/267 nm excitation pulses. In these experiments, the sample consisted of a 5.8×10^{-5} M ferrioxalate/water solution in which 0–2.5×10^{-4} M thymine was added. The radical scavenging effect was measured by the addition of 1,10-phenanthroline(phen) following the procedure described in ref 13 and 42. The optical density of the $[Fe(II)(phen)_3]^{2+}$ complex formed, which was found to be linearly dependent on the concentration of Fe(II) complex,[42] is plotted in Figure 10 as a function of the total 355 nm pulse energy. Significant decrease in the amount of Fe(II) formed was observed when 5.0×10^{-5} M thymine was added, and Fe(II) decreased even further as the amount of thymine added to the ferrioxalate solution was increased. When the concentration of thymine reached 2.5×10^{-4} M, the quantum yield of Fe(II) was found to be reduced by 63%. Both the dependence of the scavenging effect on concentration and the large, more than 50%, decrease of Fe(II) formation proves that the ferrioxalate photoreaction does not involve intramolecular ET with high quantum yield, but it is rather due to intermolecular ET between $CO_2^{\bullet-}$ and Fe(III) complex.[2,10]

(41) Ito, T.; Hatta, H.; Nishimoto, S. *Int. J. Radiat. Biol.* **2000**, *76*(5), 683–692.
(42) Tamura, H.; Goto, K.; Yotsuyan.T; Nagayama, M. *Talanta* **1974**, *21*(4), 314–318.

In summary, we propose that after excitation, the dominant reaction is Fe−O bond dissociation followed by intermolecular electron transfer. This is based on the following: (1) The Fe−O bond length changes between 0 and 140 ps including the bond increase at 2 ps and the subsequent decrease at 4–140 ps. The first intermediates formed after the excited state are assigned to Fe(III) instead of Fe(II). This assignment is supported by the experimentally found Fe−O bond length of 1.89–1.93 Å that is formed after the cleavage of two Fe−O bonds. In addition, DFT and UHF calculations predict Fe−O bond lengths of 1.90–1.91 and 1.90–1.92 Å, respectively, for the Fe(III) four-coordinated system and 2.04–2.06 and 2.01–2.02 Å for the Fe(II) four-coordinated system. (2) An large radical scavenging effect (>50%) was experimentally measured. (3) A small transient spectrum difference was observed by femtosecond spectroscopy.

3.3. Photochemical Quantum Yield. The total photoredox reaction quantum yield of ferrioxalate is about 0.60, which accounts for the reported 1.2 quantum yield for Fe(II) formation.[1] As we discussed above, there are at least two primary reaction paths that we observed after 266/267 nm excitation excluding the internal conversion back reaction: (1) formation of solvated electrons and (2) dissociation of the Fe−O bond followed by intermolecular ET. These reaction paths eventually proceed to reduce Fe(III) to Fe(II). There is no experimental evidence that shows that intramolecular electron transfer is the predominant reaction path after excitation; however, it cannot be excluded. Therefore, the mechanisms proposed based on our experimental and theoretical calculation data involve only photoelectron detachment and dissociation followed by intermolecular ET.

We have estimated the solvated electron formation quantum yield by comparing the intensity of the transient absorption band at 720 nm of ferrioxalate and ferrocyanide solutions under the same experimental conditions. Using the quantum yield of ferrocyanide which is reported to be approximately 1,[32] we estimated the quantum yield for the photodetachment of an electron from ferrioxalate to be about 0.05. In a previous study,[13] we have found that the primary photoredox reaction with either 400 or 355 nm excitation is the dissociation of ferrioxalate followed by intermolecular ET. Therefore, the quantum yield for the dissociation of the ferrioxalate after 266 or 267 nm excitation was estimated by assuming that it has the same 0.55 value as the one obtained with 405 nm excitation.[1] Considering the values of the quantum yield estimated above for both reaction paths, we determined the total photoredox quantum yield to be about 0.60, which is in agreement with the literature value obtained by Parker et al.[1] All of our experimental data and theoretical calculations point to photodissociation as the initial and dominant reaction, and it also accounts for the major structural changes that we have observed by time-resolved EXAFS. Photoelectron detachment was also found to be a primary reaction; however, because of its low quantum yield, ~0.05, it is considered as a side reaction.

According to reaction 3.2, the solvated electron reacts with ferrioxalate with a rate constant of 1.5×10^{10} M^{-1} s^{-1} to form $[Fe(II)(C_2O_4)_3]^{4-}$, whose transient absorption band is in the 400–500 nm region. However, the fast reaction of the solvated electron with ferrioxalate did not result in the formation of 400–500 nm in the picosecond to nanosecond range. This lack of the 400–500 nm band detection in this time range could be understood if we take into account the large difference between the quantum yield of the dissociation and the electron detachment, which is about 11:1. The dissociation process generates $CO_2{\bullet}^-$ radicals that are essentially responsible for the decay of the 380–500 nm band occurring in the picosecond to nanosecond range according to reactions 3.7 and 3.8. The $CO_2{\bullet}^-$/ferrioxalate reaction rate constant was estimated, from the decay lifetime of the 400–500 nm band excited by 355 nm pulses[13] to be 4.0×10^9 M^{-1} s^{-1} which is consistent with the previously reported value of 10^9-10^{10} M^{-1} s^{-1}.[23] Although the rate constant of the $CO_2{\bullet}^-$ and ferrioxalate reaction ($k = 4.0 \times 10^9$ M^{-1} s^{-1}) is about 4 times smaller than that of solvated electron/ferrioxalate reaction ($k = 1.5 \times 10^{10}$ M^{-1} s^{-1}), the absorption intensity increase at the 400–500 nm range due to the photodetachment is much smaller than the amount of decrease resulting from dissociation.

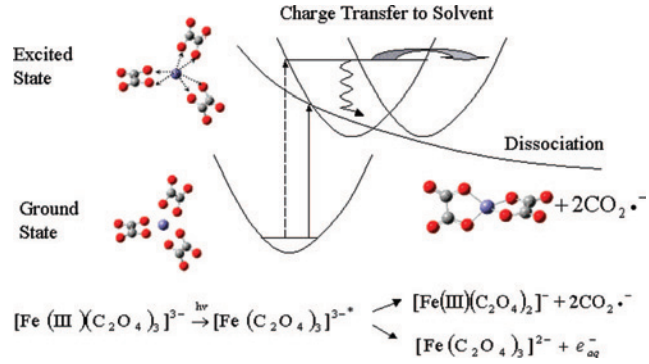

Figure 11. Diagram of electron transfer and dissociation mechanism of ferrioxalate in water.

4. Conclusion

We propose therefore, based on our ultrafast optical, EXAFS, radical and electron scavenging data, and theoretical calculations, that the ferrioxalate photoredox reaction initiated by 266/267 nm excitation to the CT band involves (1) predominantly a fast dissociation process, (2) the newly observed photoelectron detachment from ferrioxalate as a low quantum yield side reaction, and (3) subsequent reactions of e^-_{aq} and mostly $CO_2{\bullet}^-$ radical with the Fe(III) complex to reduce Fe(III) to Fe(II) by intermolecular ET. The global picture of the photoreaction paths 1 and 2, which occur after excitation, are depicted in Figure 11. However, we do not exclude a reaction that may involve intramolecular electron transfer.

Acknowledgment. This research was supported in part by the NSF, NIH, and W. M. Keck Foundation. We thank Prof. Xunliang Ding for providing the X-ray lens.

IC7016566